2021 43rd Annual International Conference of the
IEEE Engineering in Medicine & Biology Society (EMBC)
Oct 31 - Nov 4, 2021. Virtual Conference

Radiomics-based Prediction of Re-hemorrhage in Cerebral Cavernous Malformation after Gamma Knife Radiosurgery

Pei-Hsuan Kuo, Cheng-Chia Lee, Chia-Feng Lu

Abstract— **We conducted a retrospective study of long-term follow-ups in patients with cerebral cavernous malformation (CCM) treated by Gamma Knife radiosurgery (GKRS). CCM is one of the common cerebral vascular diseases. Hemorrhage is a common and dangerous symptom of CCMs, and re-hemorrhage may still occur in 30% of patients after the treatment of GKRS. We aim to identify the reliable imaging biomarkers using radiomics of magnetic resonance images (MRI) to predict the re-hemorrhage after GKRS.**

Clinical Relevance— **This study reported the longitudinal changes of MRI radiomic features in CCM after GKRS. Combining machine-learning approach with the longitudinal radiomic features can predict the re-hemorrhage of CCM after GKRS to guide the clinical management.**

I. INTRODUCTION

Cerebral cavernous malformations (CCM) are vascular abnormalities in the brain consisting of clusters of abnormal and hyalinized capillaries surrounded by hemosiderin deposits and gliosis without intervening brain tissue [1]. The incidence of CCMs ranges from 0.4% to 0.8% in the general population, but they are the most common vascular abnormality, making up 10–25% of all vascular malformations [1]. Approximately 25% of individuals with CCMs never experience any related health problems. Other people with this condition may experience serious signs and symptoms such as hemisensory deficits, cranial nerve deficits, hemiparesis, headaches, seizures, dizziness, and cerebral hemorrhage. Current treatments available for CCMs include conservative treatment, surgery, and Gamma Knife radiosurgery (GKRS). The primary therapeutic goal of GKRS is to prevent re-hemorrhage of the lesion, however about 30% of patients still experience re-hemorrhage after GKRS [2].

In this study, we developed a prediction model of re-hemorrhage after GKRS in CCMs based on longitudinal MRI radiomic features. We aim to provide a reliable system using the quantitative and non-invasive MRI method to guide the treatment decision and follow-up monitoring for the patients with CCM.

II. MATERIALS AND METHODS

A. Study Cohorts

We retrospectively enrolled 162 patients with a total of 199 CCM lesions, including 72 CCMs with re-hemorrhage after GKRS (the hemorrhagic group) and the other 127 CCMs without re-hemorrhage after treatment (the non-hemorrhagic group) from Taipei Veteran General Hospital between 1993 and 2020. Longitudinal magnetic resonance images (MRI) were collected for each patient before GKRS and yearly follow-up after GKRS. The study was approved by the local Institutional Review Board, and informed consent was waived.

The inclusion criteria of patients in this study were as follows: (i) available longitudinal data, including MRI before GKRS and annual MRI follow-ups after GKRS for at least 4 years; (ii) full series of T2-weighted images (T2W) and contrast-enhanced T1-weighted (CET1); (iii) sufficient MRI quality without significant head motion or artifacts. A total of 769 lesion-wise follow-ups were finally included for the subsequent analyses and training of re-hemorrhage prediction models.

B. Image Postprocessing and MRI Radiomics

Several postprocessing steps on the MRI were applied to reduce the discrepancy of imaging parameters using our previously published MRI radiomics platform (MRP, http://www.ym.edu.tw/~cflu/MRP_MLinglioma.html) with a graphic user interface built on MATLAB programming environment [3]. The adjustment of image resolution will be first performed to resample all voxel size to 1.00 x 1.00 x 1.00 mm^3 without gaps between consecutive slices for each MRI contrast according to Image biomarker standardisation initiative (IBSI) [4]. We also resampled all voxel size to 0.50 x 0.50 x 3.00 mm^3 without gaps between consecutive slices for each MRI contrast to evaluate the effects of anisotropic spatial resolution on radiomic analysis. The CET1 images was then registered to the subject's T2W images using a six-parameter rigid body transformation and mutual information algorithm. Image intensity normalization was employed to transform MRI intensity into standardized ranges for each imaging modality among all subjects. The CCM region of interest (ROI) was determined based on the consensus of neurosurgeons and neuroradiologists for the GKRS treatment planning according to the standard operating procedures developed by our research team. The CCM lesions were manually delineated slice-by-slice on the T2W images to generate the resultant binary lesion masks for the subsequent radiomic analysis.

The subsequent MRI radiomics analysis was also performed using the MRP [3]. An undecimated and discrete wavelet transform was employed to perform a multiscale representation of each MRI contrast using three-dimensional

PH Kuo is with Department of Biomedical Imaging and Radiological Sciences, National Yang Ming Chiao Tung University, Taipei, Taiwan (e-mail: phkuo.be08@nycu.edu.tw).

CC Lee is with Department of Neurosurgery, Neurological Institute, Taipei Veteran General Hospital, Taipei, Taiwan and School of Medicine, National Yang Ming Chiao Tung University, Taipei, Taiwan (e-mail: yfnaughty@gmail.com).

CF Lu is with Department of Biomedical Imaging and Radiological Sciences, National Yang Ming Chiao Tung University, Taipei, Taiwan (e-mail: alvin4016@nycu.edu.tw), *corresponding author.

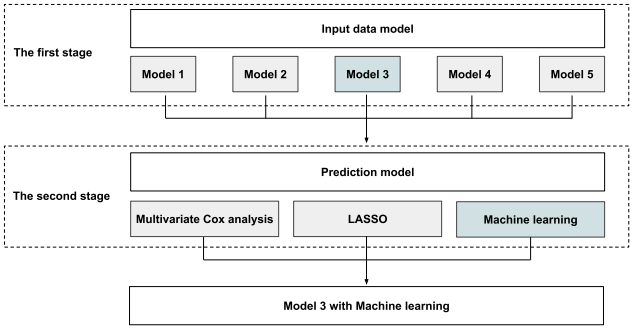

Figure 1. Two-stage process of the re-hemorrhage prediction model construction. We developed re-hemorrhage prediction model with two stages: data input models and prediction model.

Low (L) and high (H) spatial frequency filters. The 16 first-order and 73 texture features, including 22 gray-level co-occurrence matrix (GLCM) features, 11 gray-level run-length matrix (GLRLM) features, and 16 local binary patterns (LBP) features, were calculated on the raw MR images and 8 wavelet image sets (LLL, LLH, LHL, LHH, HLL, HLH, HHL, and HHH), yielding 585 features. The 8 shape and size features were calculated based on the three-dimensional geometry of the lesion volume. Overall, 1178 MR radiomics features (585 features × 2 image contrasts + 8 shape and size features) were generated for each MRI dataset.

C. Statistical Analysis of Clinical Characteristics

Even though we extracted a huge number of radiomic features from MR images that may provide comprehensive information in divulging molecular profiles of CCM, the process of feature selection that removed redundant features could potentially improve the efficacy of the re-hemorrhage prediction. Before the feature selection of radiomics features, we performed statistical analysis to identify if any clinical characteristics (age, gender, size of CCM, clinical symptoms, and GKRS treatment parameters) may be significantly different between the re-hemorrhage and non-hemorrhage groups. The clinical characteristics were divided into continuous variables and categorical variables. Continuous variables were tested by the two-sample t-test; categorical variables were tested by the Chi-square test.

D. Feature Selection and Prediction Model Construction

We developed re-hemorrhage prediction model with two stages: data input models and prediction model (**Fig. 1**). The first stage was data input model, including five sets of data input using different combinations of follow-ups. Model 1 used the last time follow-up to predict the bleeding of the next follow-up; Model 2 used the last two time follow-ups to predict the bleeding of the next follow-up; Model 3 used all of the previous follow-ups to predict the bleeding of the next follow-up; Model 4 used MRIs before GKRS and the last time follow-up to predict the bleeding of the next follow-up; Model 5 is similar with Model 4, but normalization of change values is performed. The second stage was the comparison between three prediction models, including multivariate Cox analysis, least absolute shrinkage and selection operator (LASSO), and machine-learning approaches.

Subjects were randomly divided into two subsets (70% for the training subset and 30% for the testing subset). We developed five sets of data input models. First, a 5-fold cross-validation approach with Univariate Cox analysis was used to calculate the number of repetitions of significant features (p-value less than 0.05) and rank them in order, with a maximum of 5 repetitions and a minimum of 0 repetition. Next, the significant features with at least 3 repetitions were input into the three prediction models.

We evaluated the best prediction model by accuracy, sensitivity, specificity, and the AUC of the ROC curve to determine which model had superior prediction power. After selecting the best model, we compared the prediction performance based on the isotropic spatial resolution (1.00 x 1.00 x 1.00mm^3) and anisotropic spatial resolution (0.50 x 0.50 x 3.00mm^3).

III. RESULTS

A. Clinical Characteristics of Study Cohort

Table 1 lists the clinical characteristics of 162 enrolled patients with 199 CCM lesions. Overall 59 patients with a total of 72 lesions presented re-hemorrhage after GKRS, and 103 patients with a total of 127 lesions were hemorrhage-free. Results of statistical analysis showed that no significant difference ($p>0.05$) in age, gender, size of CCM, clinical symptoms (cranial never deficits, body sensory dysfunction, hemiparesis, headache, dizziness, and seizure), average max dose, and average isodose level between the re-hemorrhage and hemorrhage-free group. Few clinical characteristics, including the lesion location and the average margin dose of GKRS, showed significant differences ($p<0.05$) between two groups. For the lesion locations, we found that brainstem and other locations are equally distributed in the hemorrhage-free group; while we found a higher value of margin dose in the re-hemorrhage group.

B. Performance of the Re-hemorrhage Prediction Models

We compared prediction performance of the fifteen re-hemorrhage models (5 input data models × 3 prediction models). The re-hemorrhage prediction model with best performance was Model 3 with machine learning of K-nearest neighbor (KNN) classifier (M3ML model). The superior performance of the accuracy, sensitivity, specificity and the area under receiver operating characteristics curve (AUC) demonstrated the capbility of longitudinal MR radiomics with the machine-learning approach for effective prediction of re-hemorrhage. The receiver operating characteristics (ROC) curves for the selected re-hemorrhage prediction models are shown in **Fig. 2**. The re-hemorrhage of CCM after GKRS can be predicted by radiomics and machine-learning approaches. For the training dataset, AUC is 1.000 and accuracy is 100.0% for predicting bleeding in the first year after GKRS; The AUC is 1.000, and the accuracy is 100.0% for predicting bleeding in the second year after GKRS; the AUC is 1.000, and the accuracy is 100.0% for predicting bleeding in the third year after GKRS; the AUC is 1.000, and the accuracy is 100.0% for predicting bleeding in the fourth year after GKRS. The detailed selected radiomic features for Model 3 with machine-learning approach are listed in **Table 2**.

TABLE 1. Clinical characteristics of 162 patients with 199 CCMs treated with GKRS between 1993 and 2020.

Characteristic	Re-Hemorrhage group	Hemorrhage-free group	P-values
No. of patients	59 (36.42%)	103 (63.58%)	-
No. of lesions	72 (36.18%)	127 (63.82%)	-
Gender (M/F)	24/35	50/53	0.3335#
Age	39.85±14.71	40.84±13.98	0.6708*
Lesion locations (count by lesion)			
Brainstem	24	61	0.0440#
Other locations	48	66	
Size of CCM (count by lesion)			
Small (< 3 cm^3)	45	88	0.6192* 0.7333#
Medium (3-6 cm^3)	13	19	
Large (> 6 cm^3)	13	20	
Clinical symptoms (count by patient)			
Cranial nerve deficits	19	28	0.4982#
Body sensory dysfunction	15	31	0.5256#
Hemiparesis	22	53	0.0818#
Headache	18	31	0.9563#
Dizziness	15	24	0.7611#
Seizure	10	11	0.2530#
GKRS Parameters (count by lesion)			
Average margin dose (Gy)	11.96±1.20	11.62±0.98	0.0290*
Average Max dose (Gy)	20.05±2.18	19.88±2.02	0.5746*
Average Isodose level (%)	59.90±5.51	58.45±6.57	0.1132*

* : Continuous variables were tested by two-sample t test

: Categorical variables were tested by Chi-square test

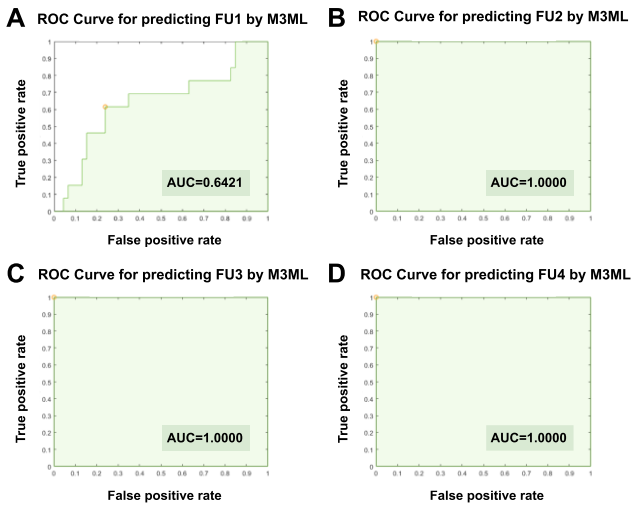

Figure 2. The ROC curves for the selected re-hemorrhage prediction model. For the testing dataset of Model 3 with machine-learning approaches (M3ML), AUC is 0.6421 and accuracy is 72.1% for predicting bleeding in the first year after GKRS (A); AUC is 1.000 and accuracy is 100.0% for predicting bleeding in the second year after GKRS (B); AUC is 1.000 and accuracy is 100.0% for predicting bleeding in the third year after GKRS (C); AUC is 1.000 and accuracy is 100.0% for predicting bleeding in the fourth year after GKRS (D), representing the satisfactory results that can be achieved in the prediction model of re-hemorrhage based on the proposed method.

TABLE 2. Radiomic predictors of Model 3 with machine-learning approaches (M3ML).

(A) Predict for the first year outcome after GKRS by M3ML
Radiomic Features
GK_CET1_HHL Texture Range
GK_CET1_HHL Texture Variance
GK_T2_LLH Texture Third quartile
GK_CET1_LHL Texture Standard deviation
GK_T2_HHL Texture Corrlation
GK_CET1_LLH Texture Third quartile
GK_T2_HHL Texture Standard deviation
GK_CET1 Texture Cluster Prominence
GK_CET1_LHL_Texture_Range
9
(B) Predict for the second year outcome after GKRS by M3ML
Radiomic Features
FU1_T2_HHH Texture_Entropy
FU1_CET1_Texture LBP First quartile
2
(C) Predict for the third year outcome after GKRS by M3ML
Radiomic Features
FU2_T2_LHH_Texture Inverse variance
GK_CET1_LLL_Texture_Energy
2
(D) Predict for the fourth year outcome after GKRS by M3ML
Radiomic Features
FU2_T2_Texture LBP Uniformity
FU1_T2_Histogram_Skewness
2

The trained prediction model was then applied to the testing dataset. The results performed on the testing dataset showed a comparable model performance with that on the training dataset suggesting the efficacy of the model.

For the testing dataset, the AUC is 0.6421, and the accuracy is 72.1% for predicting bleeding in the first year after GKRS; the AUC is 1.000, and the accuracy is 100.0%; for predicting bleeding in the second year after GKRS; the AUC is 1.000, and the accuracy is 100.0% for predicting bleeding in the third year after GKRS; the AUC is 1.000, and the accuracy is 100.0% for predicting bleeding in the fourth year after GKRS. The model performance was comparable in both the training and testing datasets for predicting bleeding in the second to forth year after GKRS (100% accuracy), except for the first-year prediction (72.1% accuracy). To improve the performance in the first-year prediction, more patients with re-hemorrhage after GKRS will be collected in our future study.

IV. DISCUSSION

We developed a re-hemorrhage prediction model, Model 3 with KNN machine-learning approach, with satisfactory performance to probe the re-hemorrhage after GKRS in patients with CCM based on MRI radiomics. The predictive score estimated by this model can predict bleeding efficiently both in the training and testing datasets for the second to fourth year. Our proposed approach could utilize information extracted from longitudinal follow-up of CCMs after GKRS

and provide a quantitative and non-invasive tool for predicting future re-hemorrhage events after GKRS.

A. Several Manifestations Related to Re-hemorrhage after GKRS

Based on our results, we identified several trends that may be associated with re-hemorrhage after GKRS. In terms of image contrast, the radiomic features extracted from the sequences used in this study (CET1 and T2W) provided useful information for the prediction of re-hemorrhage. In terms of the radiomics category, histogram and texture features showed great potential to predict re-hemorrhage, with the exception of geometry which contributed little to the prediction of re-hemorrhage after GKRS. In terms of follow-up time points, our results showed that the first two years of follow-ups provided critical information, matching the clinical decision-making strategy, to identify patients with strong recommendation for regular follow-up during the first two years after GKRS. This result was consistent with some of the literatures, while others suggested that follow-up for the first five years after GKRS was of interest.

By evaluating the effects of isotropic and anisotropic spatial resolution on predicting re-hemorrhage after GKRS, we found that the predictive performance in two different resolutions showed no significant difference.

B. Longitudinal Change of Radiomics in CCM

Figure 3 presents the longitudinal changes of MRI images in a representative patient with re-hemorrhage after GKRS and in a patient without re-hemorrhage (hemorrhage-free). According to literatures, the hemorrhagic lesions appear varied signals depending on the age of the blood products, and small fluid-fluid levels may be evident on T1W images [5]; they appear as a hypointense rim with varied signal internally depending on the age of blood products. If a recent bleed has occurred, surrounding edema may be present on T2W images, and generally no enhancement on CET1 images. In the re-hemorrhage case (**Fig. 3A**), T2W images showed a pattern consistent with the findings of previous studies. In addition, in the hemorrhage-free case (**Fig. 3B**), we found a reduction in the size of CCM lesion on both T2 images. **Figure 3C** presents longitudinal changes of the selected radiomic features in both the re-hemorrhage and hemorrhage-free cases. Since it is difficult to visualize the dynamic changes of the values in purely numerical form, we plotted a line graph to present the longitudinal changes of the radiomic features. The lines showed a relatively flat pattern in the hemorrhage-free case. However, we observed that the line in the re-hemorrhage group showed a more pronounced fluctuation before the bleeding occurrence.

Several issues and limitations are discussed as follows. First, several other MRI contrasts, including T1-weighted images, diffusion-weighted images, and time-of-flight angiography, were not available in this study. Inclusion of these MRI data may further improve the prediction performance. Second, GKRS was reported to be effective in preventing bleeding within five years after treatment, but long-term efficacy may require further study [6]. Sufficient longitudinal follow-ups and a larger number of CCM lesions should be collected in the future studies. Finally, to reduce the potential bias caused by the manual lesion delineation, the development of automatic segmentation of CCM lesions could be helpful to optimize the re-hemorrhage prediction model.

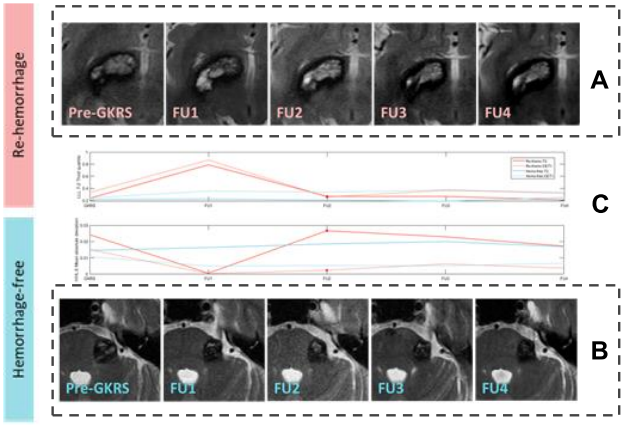

Figure 3. Longitudinal changes of images and radiomics.

The longitudinal changes of MRI images in the re-hemorrhage group **(A)** and in the hemorrhage-free group **(B)**, and the line graph of longitudinal changes of radiomic values in the re-hemorrhage group and in the hemorrhage-free group **(C)** presented the dynamic changes of CCM patterns through each follow-up.

V. Conclusions

This study investigated the longitudinal changes of MRI radiomics features in patients with CCM after receiving GKRS treatment. The combination of machine-learning approaches and longitudinal radiomic features can predict the re-hemorrhage of CCM after GKRS to guide clinical management.

Acknowledgment

This study was supported by Ministry of Science and Technology of Taiwan (109-2314-B-010-022-MY3), Taipei Veterans General Hospital, National Yang Ming Chiao Tung University, and University System of Taiwan (VGHUST110-G7-2-2).

References

[1] Dalyai RT, Ghobrial G, Awad I et al P. Management of incidental cavernous malformations: a review. Neurosurg Focus. 2011 Dec;31(6):E5.

[2] Lee CC, Wang WH, Yang HC et al. Gamma Knife radiosurgery for cerebral cavernous malformation. Sci Rep. 2019 Dec 24;9(1):19743

[3] Lu CF, Hsu FT, Hsieh KL, et al. Machine Learning-Based Radiomics for Molecular Subtyping of Gliomas. Clin Cancer Res. 2018 Sep 15;24(18):4429-4436.

[4] Zwanenburg A, Vallières M, Abdalah MA et al. The Image Biomarker Standardization Initiative: Standardized Quantitative Radiomics for High-Throughput Image-based Phenotyping. Radiology. 2020 May;295(2):328-338.

[5] Vilanova JC, Barceló J, Smirniotopoulos JG et al. Hemangioma from head to toe: MR imaging with pathologic correlation. Radiographics. 2004 Mar-Apr;24(2):367-85.

[6] Park K, Kim JW, Chung HT et al. Long-Term Outcome of Gamma Knife Radiosurgery for Symptomatic Brainstem Cavernous Malformation. World Neurosurg. 2018 Aug;116:e1054-e1059